ELSEVIER

Contents lists available at ScienceDirect

Computers and Geotechnics

journal homepage: www.elsevier.com/locate/compgeo



Moment load impact on resistance of foundation soils to seismic loads

Yeon Sam Kim, Radoslaw L. Michalowski

Department of Civil and Environmental Engineering, University of Michigan, 2028 GG Brown Bldg., Ann Arbor, MI 48109, USA

ARTICLE INFO

Keywords:
Seismic loads
Limit analysis
Bearing capacity
Generalized loads
Yield locus

ABSTRACT

The subject of the influence of the seismic excitation on limit loads of footings is revisited, with emphasis on the moment load. The kinematic approach of limit analysis is employed using two collapse mechanisms allowing footing rotation and one with pure translational kinematics. Two of the mechanisms have novel elements, not presented in earlier literature. The paper is focused on the resistance of the soil weight to activating a mechanism of failure, which can be best cast in terms of the seismic bearing capacity factor N_{γ}^{c} . Seismic loads from the superstructure are interpreted as those caused by a three-mass model, each mass with its own seismic coefficient. The notion of generalized loads is used to present the yield locus for the footing in terms of the gravity force, horizontal force, and moment. The non-symmetric components of the load are interpreted as seismically activated. The approach yields a strict upper bound to the magnitude of the load vector causing failure. Of the three failure mechanisms considered none yields the best (least) solutions for all combinations of loads. In general, the two mechanisms with footing rotation perform better for large moments, whereas the translational mechanism yields better results when moments are small. However, even in the absence of a moment load, the rotational mechanism can yield better estimates of the limit load when the seismic coefficient is relatively large.

1. Introduction

Structures affected by ground motion in seismic regions are subjected to inertial loads which must be transferred to the foundation soil, in addition to gravity loads. Similarly, the distributed gravity load in the soil will be amended by distributed inertial forces, leading to an overall complex loading of the foundation soil. As the ground motion is time-dependent, the inertial loads are dependent on time. Collapse of a foundation footing is predicated on the formation of a failure mechanism in the foundation soil, and the design of footings requires selecting a size large enough to prevent the formation of the plastic mechanism. The design requires selecting an appropriate load combination that includes both the gravity and inertial loads. The latter are time-dependent, but a customary approach is to consider both to be steady, with the inertial load components in some proportion to the peak acceleration of the ground motion.

The findings in this study are useful in both the safety assessment of footings subjected to combined, non-symmetric static loads, and to loads induced by ground shaking during seismic excitation. In the presentation of the results emphasis is placed on the latter, as the impact of the moment load induced by the superstructure subjected to shaking is often overlooked when considering seismic load combinations. A part of the

novelty in this paper is in the interpretation of the multiplicity of seismic load combinations, even though a detailed dynamic analysis of the superstructure is not attempted.

The early attempts solving for seismic bearing capacity of strip footings considered both the superstructure and the foundation soil to be subjected to the same seismic acceleration (e.g., Sarma & Iossifelis, 1990, Richards et al., 1993). This approach ignores phenomena such as ground motion amplification and a variety of possible motion-induced load combinations from the superstructure. The differences in motion phase on different components of a structure were ignored in the early studies, and even more importantly, the impact of the seismically induced moment load on a footing was not accounted for in these early efforts. Attempts to take moment load into account have been made mainly in offshore foundations, but not necessarily in the context of ground motion. When interpreting the failure state of a footing, a limit state envelope involving interaction of vertical, horizontal and moment loads can be adopted as in the concept of generalized loads and velocities introduced by Prager (1959) to analyze structures such as beams, frames and plates. This path will be explored in this paper.

The tools used in the early approaches to seismic bearing capacity were the *limit equilibrium method* and *kinematic limit analysis*, the latter rendering a rigorous upper estimate to the bearing capacity of strip

E-mail addresses: yeonsam@umich.edu (Y.S. Kim), rlmich@umich.edu (R.L. Michalowski).

^{*} Corresponding author.

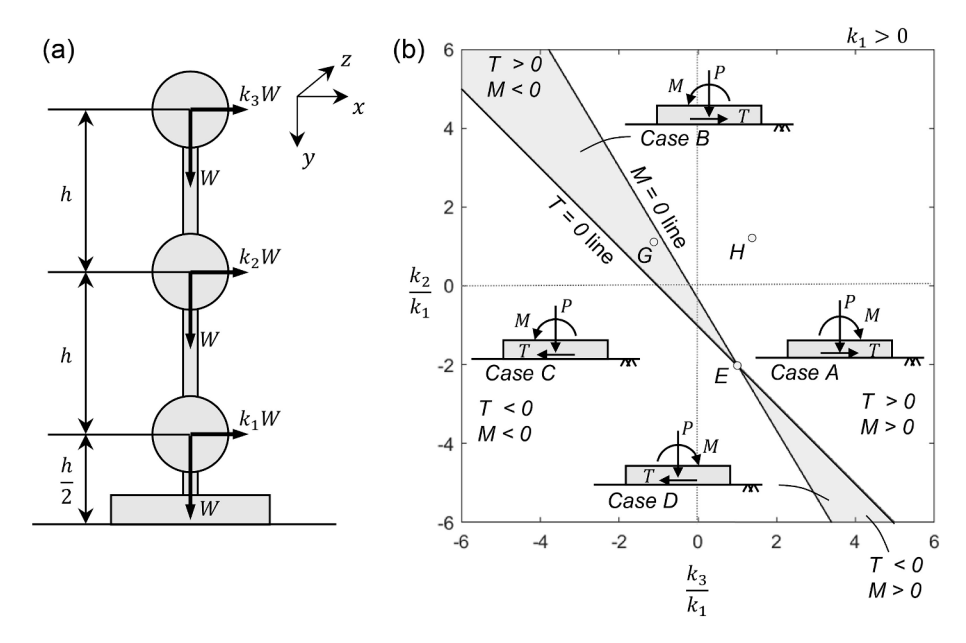


Fig. 1. (a) Schematic of a three-mass model of the superstructure, and (b) load combinations governed by combinations of mass accelerations.

footings subjected to seismic loads. There is substantial literature available regarding the capacity of soils to carry non-symmetric loads, though many of the papers relate to loads that are not necessarily caused by seismic events. For example Nova & Montrasio (1991) and Gottardi & Butterfield (1993) developed yield loci in terms of generalized load on a footing that included independent force components and moment. Salençon & Pecker (1995) provided upper and lower estimates of limit loads including inclined and eccentric forces on footings resting on undrained soils. Analyzing the impact of seismic loads on resistance of non-cohesive soils, Dormieux & Pecker (1995) indicated that while the major influence comes from the structural loads, the soil inertial load should not be neglected. Using earlier developed mechanisms, Paolucci & Pecker (1997) presented seismic limit loads for footings with inclined and eccentric loads. They also indicated that the impact of the inertial loads from the superstructure is more significant than that from the soil inertia. Non-symmetric loads on foundation soils were the subject of research related to offshore structures. Bransby & Randolph (1998) constructed the yield locus for offshore skirted foundations in the general load space. Soubra (1999) provided seismic bearing capacity factors using a simple multi-block mechanism in kinematic limit analysis, though omitting the impact of moments. Hjiaj et al (2004) used finite element limit analysis to obtain solutions to bearing capacity of footings on Mohr-Coulomb soils under inclined loading.

More recent investigations of the subject recognize that during earthquake shaking the accelerations affecting the superstructure and the foundation soil are not the same (Cascone & Casablanca, 2016; Pane et al., 2016). These newer studies also employ numerical methods to search for the bearing capacity of footings subjected to seismic loads, such as finite element analysis and the finite difference approach. To avoid a large number of charts with bearing capacity for a variety of different load combinations, both Pane et al. (2016) and Cascone & Casablanca (2016) used the concept of an *influence factor* or a *seismic reduction factor*. This made it possible to isolate the effect of seismic lateral loads of the superstructure from the effect of soil shaking. However, such a procedure needs to be exercised with caution as it uses a superposition of different effects, which is not universally permissible when the behavior of the system is non-linear.

In his note on the seismic effects on footings resting on undrained soils, Pender (2018) brought up an interesting observation indicating the negligible impact of soil shaking on the bearing capacity of undrained soils. This aspect, however, does not fall under the purview of

this paper, as it focuses on pressure dependent soils without any cohesiveness. This introduction is to provide some background to the study presented, but it is not meant to be a comprehensive literature survey; for a more detailed bibliography of the subject, the reader is directed to the list of references in the paper by Pane et al. (2016).

This paper introduces novel elements into the seismic bearing capacity analysis, in particular, the direct consideration of the seismic moment in bearing capacity analysis; it explores new mechanisms of foundation soil failure, and it identifies the specific regions on the yield locus associated with the specific modes of foundation soil failure when subjected to non-symmetric loads.

2. Problem statement

The resistance of foundation soils to loads is typically considered as a superposition of three components: first, the soil cohesiveness and the effort needed to overcome the shear resistance of soil during formation of a plastic mechanism; second, the resistance of the overburden that needs to be displaced if the failure is to take place; and third, the component owed to the soil gravity force opposing the failure. The minima of the three resistance components are typically calculated independently and the superposition is used to determine the total capacity of footings to carry the loads. This method, attributed to Terzaghi (1943), though earlier suggested by Keverling Buisman (1940), uses an approximation allowing the three components to be determined using different collapse mechanisms. While this introduces some inconsistency into the solution, such an approach is conservative, as the sum of the three minimum resistance components cannot be larger than the minimum of their sum.

This paper is focused only on the resistance of the foundation soil weight to carry gravity loads and inertial forces from the superstructure, as well as the inertial forces induced in the soil by shaking. Despite of the dynamic character of the seismic forces, they will be considered steady loads in the analysis. Horizontal inertial forces, associated with propagation of S-waves, will be considered, but the vertical shaking will be ignored in the analysis as they are induced by P-waves of a different frequency (Gazetas et al., 2009). The overburden and the cohesiveness of the soil are not considered in this study, however a full array of inplane loads is considered. The outcome sought in this study is best characterized by factor $N_{\gamma}^{\rm s}$ used in the three-term bearing capacity expression, accounting for the impact of seismic loads. The mechanisms

utilized in this study allow addressing the bearing capacity components owed to the soil cohesion and overburden by including appropriate work rate terms in the work balance equation, but the influence of cohesion and overburden was not part of the study.

The strength of the soil is described by the pressure-dependent Mohr-Coulomb function with its deformation governed by the normality flow rule. The scale of the problem is defined by the width of a long footing, and the plane-strain solution to the problem in terms of generalized limit loads (two components of the force and a moment) will be sought.

The method selected for solving the problem is the kinematic approach of limit analysis. This method is predicated on the normality flow rule and the convexity of the yield criterion of the soil. It uses a theorem, which can be conveniently stated as follows: the rate of internal work in any kinematically admissible mechanism is not smaller than the work rate of true external loads in that mechanism

$$\int_{V} \sigma_{ij}^{k} \dot{\varepsilon}_{ij}^{k} dV + \int_{I} T_{i}^{k} [v]_{i}^{k} dL \ge \int_{S} T_{i} \nu_{i}^{k} dS_{t} + \int_{V} X_{i} \nu_{i}^{k} dV \tag{1}$$

The two terms on the left-hand side include the rate of internal work in the continually deforming soil and along the velocity discontinuities, and the right-hand side represents the work rate of external forces, with T_i being the boundary stress and X_i is a volume-distributed load, such as the gravity load. The consequence of this theorem is that an active limit load calculated using any kinematically admissible mechanism is a strict upper bound to the true load causing failure. The most accurate upper bound to the active limit load is found from a mechanism that yields the minimum of the load. This requires selecting a mechanism that is sensitive to the loads involved and optimizing its geometry to arrive at the least upper bound.

3. Loads

The most common approach to the assessment of seismic load capacity of footings has been based on using a quasi-static load, in some relation to the peak acceleration of the ground motion, as alluded to earlier. In addition, a strong assumption is made typically that the horizontal acceleration affecting the superstructure is in phase with the acceleration in the foundation soil, with matching magnitudes of accelerations. In the following we will concentrate first on interpretation of possible loads transferred to the footing from the superstructure, but without a dynamic analysis of the latter. Fig. 1(a) shows schematically a superstructure modeled as three equal masses m. As a result of the dynamic motion of the footing and the structure, the three masses are allowed to move with different horizontal velocities and accelerations, but no vertical motion is included. Different combinations of motion of the three masses are considered allowing multiplicity of combinations of horizontal seismic force and a moment on the footing. This 3-mass model was selected as it is the least complex model allowing the seismic forces or seismic moments (or both) on the superstructure to cancel out for non-trivial combinations of mass accelerations. The authors are not aware of such a model being used by others to interpret possible combinations of seismic loads.

Each mass in the model produces gravity load W, with total gravity load on the footing being P=3 W. Assume each mass being subjected to a different horizontal acceleration, defined by a respective seismic coefficient k_i (i=1,2,3). Finding these accelerations in relation to the ground motion would require a detailed dynamic analysis of the superstructure. However, this structural example model is used here only to demonstrate that different combinations of horizontal accelerations lead to distinctly different combinations of loads, with the potential failure mechanism being dependent on that combination. For the topology of the system in Fig. 1(a), horizontal seismic load T and seismic moment M transferred to the foundation footing are

$$T = W(k_1 + k_2 + k_3) = 3Wk = Pk$$

$$M = \frac{1}{2}Wh(k_1 + 3k_2 + 5k_3) = \frac{1}{6}Ph(k_1 + 3k_2 + 5k_3)$$
(2)

where W is the weight associated with each mass, and k is the average of the three mass seismic coefficients: $k = (k_1 + k_2 + k_3)/3$. The conditions for the loading combination T > 0 and M < 0 (see coordinate system in Fig. 1) are easily found from inequalities $k_1 + k_2 + k_3 > 0$ and $k_1 + 3k_2 + 5k_3 < 0$, leading to the following set of two inequalities

$$\frac{k_2}{k_1} > -\frac{k_3}{k_1} - 1$$

$$\frac{k_2}{k_1} < -\frac{5k_3}{3k_1} - \frac{1}{3}$$
(3)

The criteria in Eq. (3) are plotted in Fig. 1(b) as two straight lines, and they discriminate between two distinct types of loading indicated by the inserts in Fig. 1(b), marked as load combinations A and C for which $sgn(T \cdot M) = +1$ and loads B and D for which $sgn(T \cdot M) = -1$.

Thus a rich variety of loads is theoretically possible, out of which the realistic combinations would follow from a dynamic analysis of the superstructure interacting with the ground motion. It is hypothesized that the two distinct types of loading (A, C and B, D) are likely to induce different failure mechanisms in the foundation soil. The two inequalities (3) plotted as lines in Fig. 1(b) represent seismic loads with either zero horizontal force or zero moment. Their cross-section at E defines a combination of the three seismic coefficients $(k_2/k_1=-2,\,k_3/k_1=1)$ where, despite non-zero accelerations, no inertial load from the superstructure is transferred to the footing. In the analysis of bearing capacity, seismic coefficients k_1, k_2, k_3 are distinct from the seismic coefficient applied to the soil, k_3 .

The footing loading classified as A and C were considered earlier, for example, by Paolucci & Pecker (1997) and Michalowski & You (1998a), whereas loads B and D were addressed to a lesser extent (Narita & Yamaguchi, 1989; Michalowski & You, 1998a), and a new failure mechanism was developed in this study to capture a better upper bound solution to limit loads B and D. While the dynamic analysis of the superstructure was not attempted, the distinction between different load combinations in Fig. 1(b) are likely to be associated with the modal response of the structure to seismic excitation. Load combinations denoted as B and D may occur for higher-order modes that are likely to be associated with vibration periods corresponding to larger spectral accelerations. Loads B and D are likely to be dependent not only on the structural response, but also on the frequency content of the ground motion.

When the three masses in Fig. 1(a) are subjected to horizontal accelerations, the induced lateral inertial forces will be transferred directly to the soil through a mat foundation or will be distributed across an array of spread footings. However, a portion of the seismic moment produced by the horizontal inertial forces in the superstructure may be transferred to the foundation soil as vertical force-couples on pairs of spread footings, causing an increase/decrease in vertical forces on individual footings (not disturbing the total vertical gravity load from the superstructure), and only a small portion of the moment may transfer as moments on individual footings. Assessment of seismically-induced loads transferred from the superstructure to the foundation soil is not a subject of this paper. Rather, it is the non-symmetric combination of limit loads on a footing that is of interest here, as well as indicating how the seismic loads may relate to the generalized yield criterion (yield locus). Special attention will be paid to possible variation in failure modes (collapse mechanisms), dependent on the combination of loads. The use is made of a three-dimensional interaction surface, or the generalized yield condition (Prager, 1959).

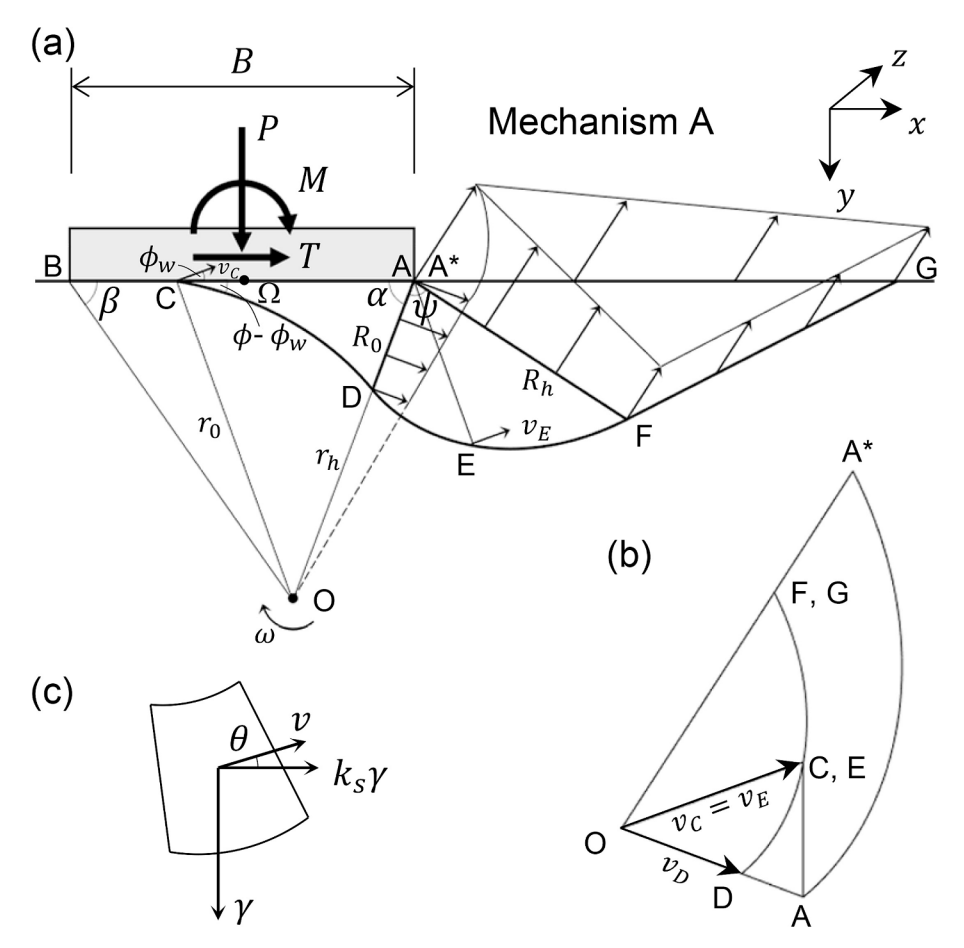


Fig. 2. Mechanism A (combined rotation-translation failure): (a) collapse mechanism, (b) hodograph, and (c) example volume element in region ADFA used for calculating the work rate of gravity and seismic forces in the soil.

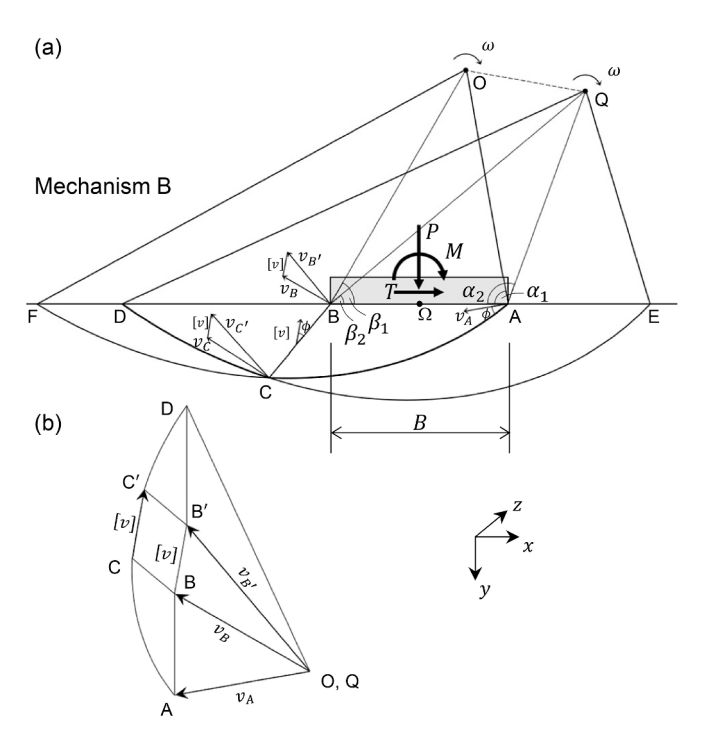


Fig. 3. Mechanism B (dual-rotation collapse): (a) mechanism, and (b) hodograph.

4. Plastic mechanisms

Three mechanisms of soil collapse are considered. The basic load, in the absence of seismic shaking, is the gravity load from the superstructure. The inertial forces induced by shaking in the soil and in the superstructure contribute to the loss of symmetry in the loading. First the load from the superstructure alone is considered. Because the inertial loads are treated as steady, finding the limit combinations of non-symmetric loads with inertial components, in addition to gravity loads, is no different than finding a generalized yield locus for a footing loaded with combinations of non-symmetric static loads, including moment M, horizontal force T, and vertical force P.

Combinations of positive and negative forces and moments are illustrated graphically in Fig. 1(b) in order to distinguish among different combinations of loads. In the following three figures illustrating three plastic mechanisms, all loads are marked as positive, consistently with the coordinate system used and shown in the figures.

The first mechanism is shown in Fig. 2 and it will be referred to as Mechanism A. It encompasses a rotating portion, including the footing and soil region CDAC beneath, both rotating about point O with angular velocity ω . The soil internal friction angle is ϕ and the footing-soil interface friction angle is ϕ_w . Velocity v_C at point C is inclined at angle ϕ to kinematic discontinuity CD, and at ϕ_w to the footing-soil interface, conforming to associativity of plastic deformation. As region CDAC rotates as rigid, line CD is a log–spiral section of kinematic discontinuity CDEFG.

As line CDEFG is smooth, no other discontinuities are present in the mechanism. Point D is an inflection point, and while OC and AE are parallel, velocities v_C and v_E are parallel and equal in magnitude. Point A

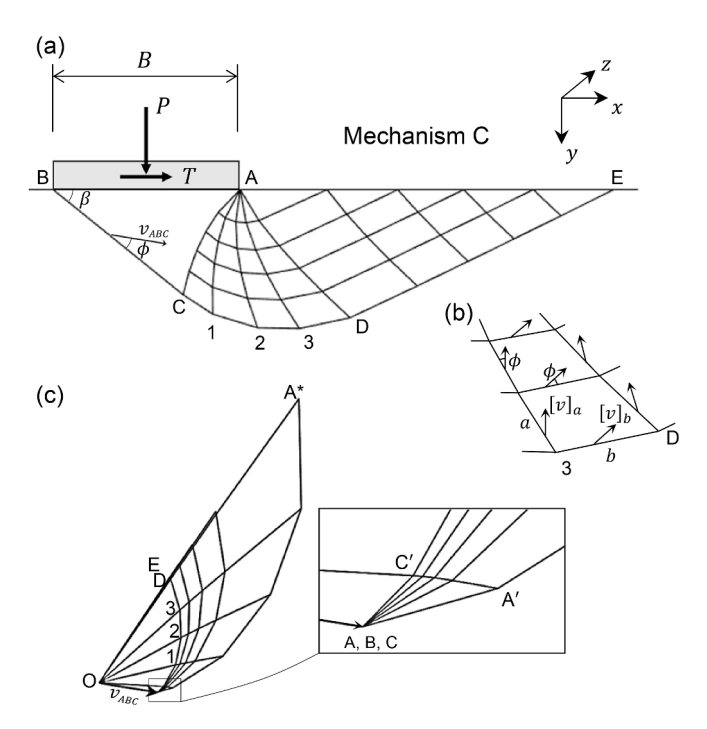


Fig. 4. Mechanism C (multi-block translation pattern): (a) mechanism, (b) fragment of multi-block mesh, and (c) hodograph.

is a singular point and line DEF is a log-spiral, but region ADEFA is subjected to continual shear (not rigid rotation). The velocity at point A spans a fan of velocities changing in magnitude and direction, illustrated in the hodograph as log-spiral AA*, Fig. 2(b). Finally, triangular region AFGA is subjected to a combination of translation and simple shear. Velocities in the entire mechanism are illustrated in the hodograph shown in Fig. 2(b).

The mechanism in Fig. 2(a) is fully defined by 3 independent variables, for example, two coordinates of center of rotation O and angle ψ . However, as the geometry of the mechanism needs to be optimized in order to obtain the best (the least) estimate of the limit load, it is more convenient to select three angles as the independent variables, and angles α , β , and ψ were selected. This mechanism is similar to that used by Salençon & Pecker (1995) for undrained soils, and it was used earlier for analyzing spread footings on drained soils subjected to combined loads (Michalowski & You, 1998a); it is utilized here to consider nonsymmetric loads in the context of seismic impact.

The second mechanism is illustrated in Fig. 3. It shows a dual-rotation motion pattern, and it will be referred to as Mechanism B. This mechanism has not been considered in earlier literature. It consists of two soil blocks rotating about separate centers O and Q, separated by planar velocity discontinuity surface BC originating from footing corner B. Block ACBA rotates about point O with angular velocity ω . The second block, BCDB, rotates with velocity ω about point Q. Curve AC is a section of log-spiral ACF, and CD is a section of log-spiral ECD.

As the motion of the two blocks is defined by rotation about two different centers, planar surface BC separating the two blocks is a kinematic discontinuity with velocity jump vector $[\nu]$, perpendicular to a line passing through O and Q. The plastic mechanism is separated from the soil at rest with kinematic discontinuity ACD (ACD has a discontinuous derivative at C). Velocities in Mechanism B are illustrated in the hodograph in Fig. 3(b). The mechanism in Fig. 3(a) is fully defined by 4 independent variables, for example, the coordinates of rotation centers O and Q. It was convenient to define points O and Q using two sets of angles: α_1 , β_1 , and α_2 , β_2 , as illustrated in Fig. 3(a). Note that once rotation centers are defined, only one point C exists on log-spiral ACF that renders the mechanism admissible. This point is found from the

condition that velocity jump vector $[\nu]$ on BC must be orthogonal to line passing through points O and Q.

Both Mechanism A and Mechanism B provide rotation of the footing, making them sensitive to the seismic moment load. However, the two of them are likely to deliver a better bearing capacity under different load conditions, *i.e.*, Mechanism A is expected to be more effective with loads marked A and C in Fig. 1(b), whereas Mechanism B is expected to yield a better (lower) limit load under load combinations B or D (*i.e.*, where force T in Fig. 3(a) is negative).

The third mechanism considered is purely translational, with the footing and block ABCA moving with unique velocity v_{ABC} , Fig. 4(a). This mechanism is not sensitive to moment loads, as the work of the moment on pure translation is nil, but it is sensitive to the seismic horizontal load, and it is expected to yield the best solution under some combinations of loads, particularly those with small or zero moment. Adjacent to block ABCA is a group of blocks contained by piece-wise linear curves AC and AD. Except for the triangular blocks sharing common singular point A, all other blocks in that region are quadrangles. Each block moves as rigid with its own velocity, and it is separated from adjacent blocks with straight-line kinematic discontinuities, as illustrated in Fig. 4(b). The velocity field in region ADEA has two distinct families of piece-wise linear kinematic discontinuities, which divide the field into rigid blocks. The hodograph in Fig. 4(c) illustrates the block velocities and the discontinuity vectors at their interfaces. Inclination of each straight-line segment of a velocity discontinuity is governed by its own angle that is an independent variable constrained by kinematic admissibility of the mechanism. The number of independent variables in Mechanism C then depends on the number of blocks. If the total number of blocks is n and the number of blocks bordering block ABCA along piece-wise linear flank AC is a, then the total number of independent variables can be found from formula 2(n-1) + a. This formula includes a-1 variables needed to define the location of points along AC. For example, the mechanism in Fig. 4 has 36 blocks, and the number of independent variables is 2(36-1) + 5 = 75.

5. Results

5.1. Calculating limit loads

The purpose of this study is to determine the yield locus of the footing in terms of generalized loads (two components of the force and a moment), and indicate how this locus relates to different modes of failure and to possible seismic loads. No cohesion in the soil and no overburden are considered, and the study is focused on the resistance of the soil weight to carry non-symmetric loads. This part of foundation soil resistance to load is typically contained in bearing capacity factor $N_{\gamma}^{\rm s}$ (here with superscript s); therefore, the yield locus in the load space will be developed first, and then charts will be shown with factor $N_{\gamma}^{\rm s}$ for some range of internal friction angle of the soil and some variation of non-symmetric load characteristics.

The upper bound to an active force causing failure of a structure can be calculated from the theorem in Eq. (1). Application of this inequality is straightforward for a single-parameter loading, but in general, the footing can be loaded with three independent loads: vertical force P, horizontal force T, and moment M. If the non-symmetry of loading is introduced by the seismic action alone, then both T and M can be cast as functions of gravity load P and the characteristics of the ground motion as well as those of the superstructure, as indicated in Eq. (2). However, finding mass accelerations in the model requires dynamic analysis of the structure, which is beyond the scope of this study. Consequently, the calculations will be performed for a given horizontal acceleration K applied to the superstructure (average of seismic coefficients of all masses in the superstructure model) and given moment through enforcing constant eccentricity of the gravity load. Such loads can be interpreted as contained within two planes in load space P, T, M, as

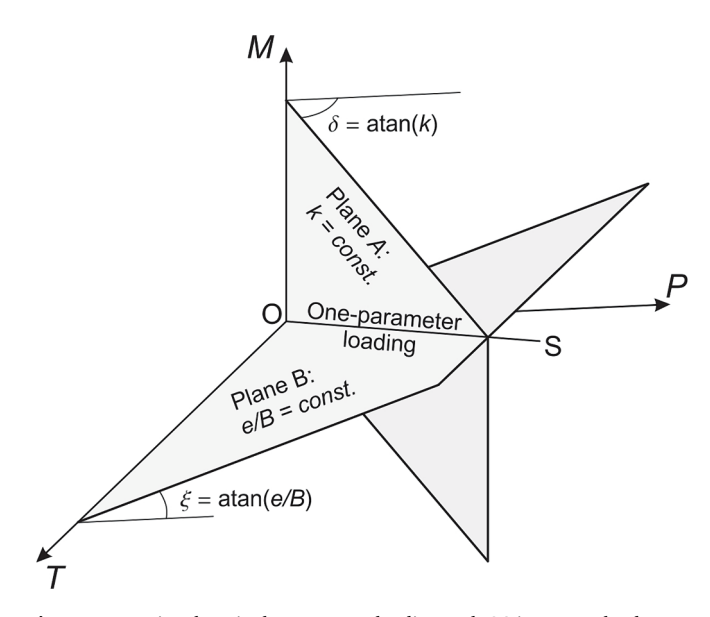


Fig. 5. Proportional or single-parameter loading path OS in P, T, M load space.

illustrated in Fig. 5. The cross-section of the two planes illustrates the proportional, one-parameter loading path. Consequently, using Eq. (1) one can formulate a problem with given k and e/B, and one unknown, namely the upper bound to limit vertical load P. A solution to this problem yields one point on a surface in the P, T, M space, referred to as the footing's yield locus. This surface determines the combinations of loads P, T and M that define the limit state of the footing. One needs multiple calculations for a variety of k and e/B combinations to obtain multiple points on the yield locus allowing construction of the entire surface. In the following, this process is described for the specific problem in this paper.

Because no cohesion is considered in the soil, the normality flow rule predicts no work dissipation in the soil, and the left side of inequality (1) becomes zero, consequently

$$\int_{S_t} T_i \nu_i^k dS_t + \gamma \int_V n_i \nu_i^k dV \le 0$$
(4)

Superscript k refers to the kinematically admissible velocity field. The first term in inequality (4) includes all loads on the footing (T_i being the stress vector on the footing-soil interface S_t), whereas the work rate of the soil weight is described in the second term (with n_i being the unit vector in the direction of gravity). This term can be evaluated in any mechanism by taking a volume integral of expression $\gamma v (-\sin\theta + k_s \cos\theta)$, where γ is the soil unit weight, v is the magnitude of the velocity vector, k_s is the seismic coefficient in the soil, and θ is illustrated in Fig. 2 (c). Considering Mechanism A in Fig. 2(a), components of the velocity vector of the footing center Ω are: $v_x^\Omega = \omega l \sin\beta$ and $v_y^\Omega = \omega (B/2 - l \cos\beta)$, where l is distance OB in Fig. 2(a). Inequality (4) can now be written for Mechanism A as

$$Pv_y^{\Omega} + Pkv_x^{\Omega} + Pe\omega + \gamma \int_V \nu(-\sin\theta + k_s \cos\theta) dV \leq 0$$
 (5)

oı

$$P \leq \frac{-\gamma \int_{V} \nu \left(-\sin\theta + k_{s}\cos\theta\right) dV}{\nu_{y}^{\Omega} + k \nu_{x}^{\Omega} + e \,\omega} = \frac{\gamma \int_{V} \nu \left(\sin\theta - k_{s}\cos\theta\right) dV}{\omega \left[\frac{B}{2} - l(\cos\beta - k\sin\beta) + e\right]}$$
(6)

where V is the volume of the entire mechanism CDEFGAC, k is the average seismic coefficient as defined in Eq. (2), and k_s is the seismic coefficient applied to the foundation soil. The right-hand side of inequality (6) yields the upper bound to the limit of one-parameter

loading P calculated using Mechanism A. All velocities in the mechanism are linear functions of order one of angular velocity ω , hence the estimate of P is independent of ω .

Following the same procedure, the respective expressions were developed for the remaining two mechanisms. The formula for Mechanism B is developed in the Appendix A, and given in Eq. (15), whereas the following expression was developed for Mechanism C

$$P \leq \frac{\gamma \sum_{j=1}^{n} \nu_{j} (\sin \theta_{j} - k_{s} \cos \theta_{j}) \Delta V_{j}}{\nu_{ABC} [\sin(\beta - \phi) + k \cos(\beta - \phi)]}$$
(7)

where n is the number of blocks in the mechanism, v_{ABC} is the velocity magnitude of the block immediately beneath the footing, θ_j is an angle that velocity of block j makes with axis x (measured counterclockwise), β is an angle (independent variable) shown in Fig. 4(a), and v_j and ΔV_j are the velocity magnitude and the volume of block j, respectively.

The details of optimizing the mechanisms in order to obtain the least upper bounds to the limit loads on footing are given in Appendix A.

5.2. Yield locus

Points on the yield locus are determined by the mechanism yielding the least limit load vector in load space P, T, M. It was convenient to find points on the yield locus by a series of computations for constant average superstructure seismic coefficient k (stationary plane A in Fig. 5), with varied moment or eccentricity e of force P (varied plane B, defined by angle ξ in Fig. 5).

First, the footing yield locus was determined for the case with the seismic load from the superstructure alone ($k \neq 0$) and no seismic load in the soil ($k_s = 0$). This yield surface then is no different than the surface for static non-symmetric limit loads, and it is shown in Fig. 6(a). The yield locus is shown in the dimensionless load space $P/\gamma B^2$, $T/\gamma B^2$, $M/\gamma B^3$. The internal friction of the soil was taken in calculations as $\phi = 30^\circ$; no bonding on the footing-soil interface was considered, and the interface friction angle was taken in the amount of 2/3 of ϕ , i.e., $\phi_w = 20^\circ$.

The red portion of the surface shows the region governed by the rotation-translation Mechanism A. As the limit analysis was employed, deformation of the soil in the analysis was governed by the normality flow rule. Consequently, the yield locus in terms of loads P, T, and M is the plastic potential for generalized velocities, here two components of displacement velocity and a rotation (angular velocity) of the footing. Generalized velocities are illustrated by vectors \dot{p} orthogonal to the yield locus. As the yield locus is presented in the dimensionless space, the generalized velocity components reside in the conjugate velocity space with coordinates multiplied by the respective norms used to produce the dimensionless load space.

The rotation appears to be the dominant velocity component in the upper-middle portion of the yield locus. Point H indicates a point with loads caused by seismic action with coefficients k_1 , k_2 , k_3 , defined by point H in Fig. 1(b), with coordinates k_2/k_1 , k_3/k_1 , of 1.4 and 1.2, respectively, $k_1=0.056$ and the 3-mass superstructure model characterized by h/B=0.988.

The gray vertical surface in Fig. 6(a) is associated with the failure mode in Mechanism C. This section of the yield locus is parallel to the moment axis, and generalized velocity vector \dot{p} is parallel to plane T, P, i. e., it does not have an angular velocity component. This is consistent with the purely translational mode represented by Mechanism C. The edge where the two sections intersect does not have a unique derivative. A point on this edge indicates a yield load point with non-unique deformation, where the location of rotation center O in Fig. 2(a) moves deeper and deeper into the soil, causing the plastic Mechanism A to transform progressively into translational Mechanism C, the case interpreted by Koiter (1953) with his flow rule applicable to singular points on the plastic potential.

Portions of the yield locus in Fig. 6(a) marked as blue show the combinations of the loads causing the footing failure illustrated by

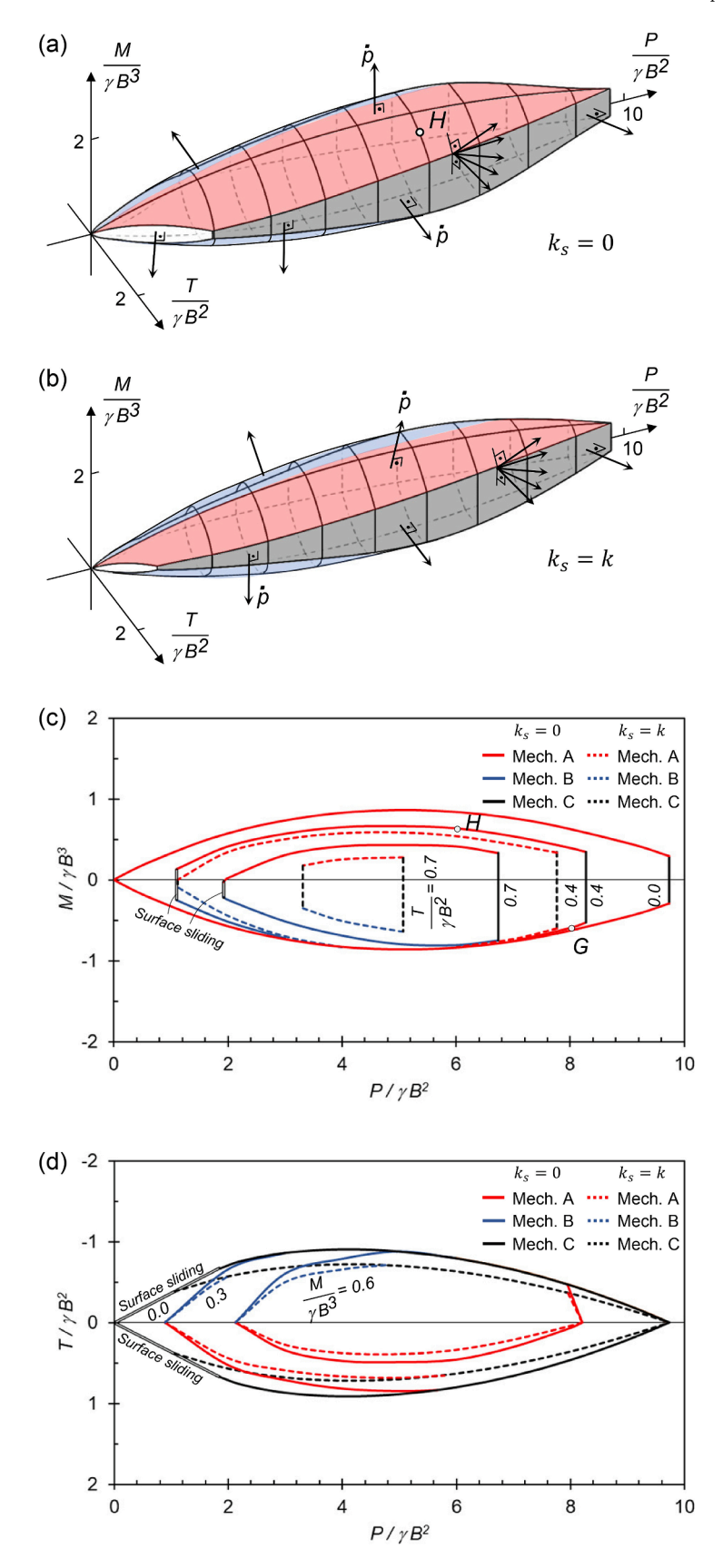


Fig. 6. Yield locus for a strip footing: (a) non-symmetric load from superstructure only $(k \neq 0, k_s = 0)$, (b) both superstructure and the soil subjected to inertial forces $(k_s = k \neq 0)$, (c) cross-sections T = const., and (d) cross-sections M = const.

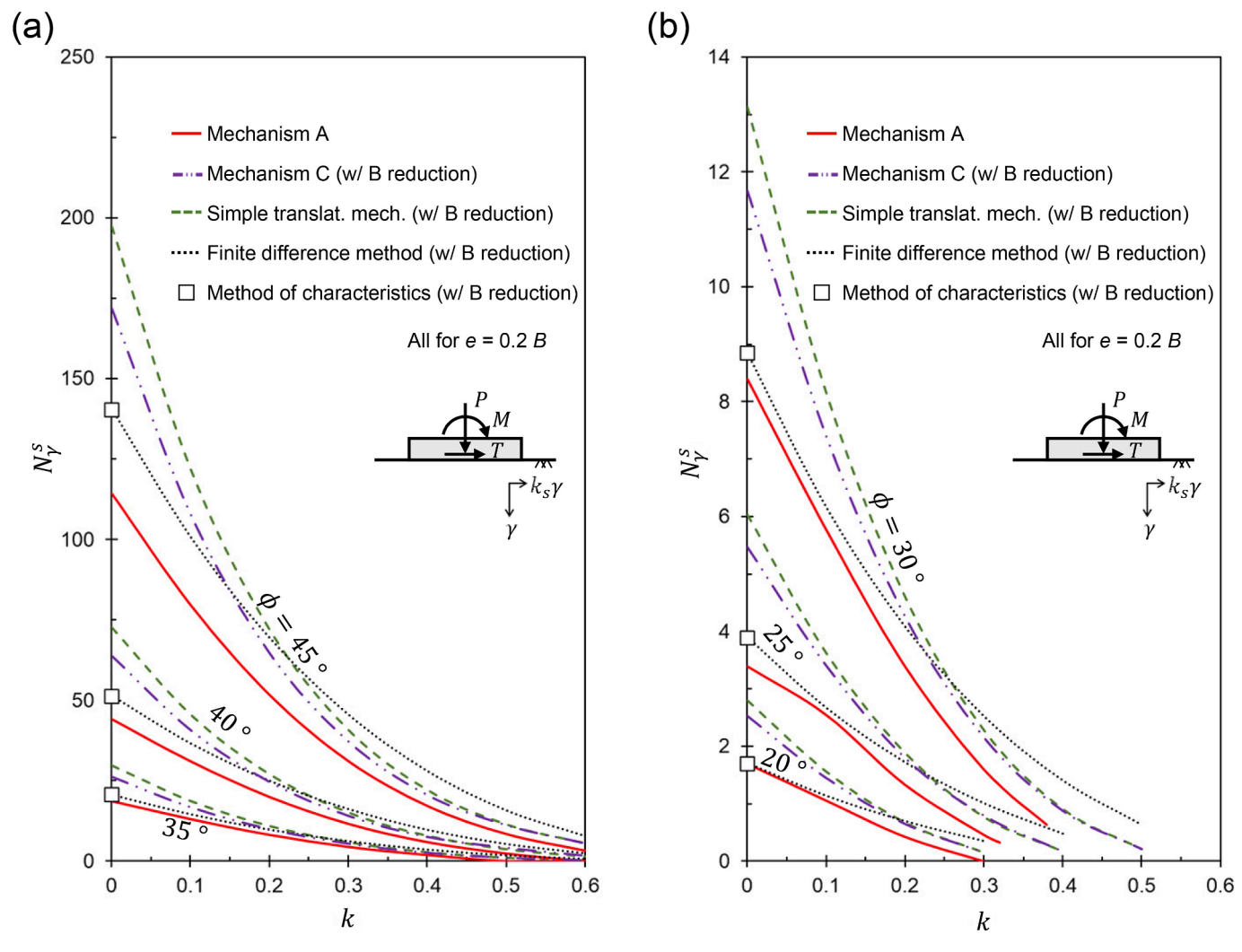


Fig. 7. Factor N_x^s for constant eccentricity e/B = 0.2 and $k_s = k$.

Mechanism B in Fig. 3(a). These sections of the surface reside predominantly in regions where the product of the moment and the horizontal force is negative, $sgn(T \cdot M) = -1$ (see also shaded areas in Fig. 1(b)). These regions are mostly obscured in the view of the first octant of the load space in Fig. 6(a).

A small white oval region close to the origin of the load space is associated with surface sliding of the footing. Because the normality flow/sliding is enforced, the sliding vector (normal to the yield locus) is not parallel to the horizontal footing-soil interface, but has a dilative component. There is a short interface (edge) on the yield locus where the regions associated with surface sliding (white) and translational Mechanism C (gray) join. The derivative along this edge is not unique, indicating that either surface sliding or translational mechanism can occur for the same load combination. Terminal points of this edge are then singular points where, in addition, the kinematics of failure consistent with either Mechanism A (when M > 0) or Mechanism B (when M < 0) can be activated.

The impact of the seismically activated inertial force in the soil is illustrated in Fig. 6(b). The case considered is one with seismic coefficient in the soil k_s equal to the average seismic coefficient k in the 3-mass model. Not surprisingly, the yield locus accounting for seismic coefficient in the soil is leaner than that in Fig. 6(a).

Cross-sections of both yield loci with planes $T={\rm const.}$ are shown in Fig. 6(c). Red, blue and black relate to the three mechanisms A, B, and C, respectively. Solid lines show cross-sections with no seismic acceleration in the soil, $k_{\rm s}=0$, whereas the dashed lines indicate cross-sections where

 $k_{\rm S}=k$. Vertical segments ($P={\rm const.}$) of the cross-sections indicate kinematics consistent with either translational mechanism C or surface sliding. Both point H and point G are on the cross-section $T/\gamma B^2=0.4$, with G defined for combination $T\cdot M<0$, for which Mechanism B yields the least failure load. Point G can be identified on the graph in Fig. 1(b) as $k_2/k_1=1.1$, $k_3/k_1=1.2$, with $k_1=0.167$ and the 3-mass superstructure model characterized by h/B=1.543.

Fig. 6(d) shows cross-sections of the two yield loci with planes of constant moment. It is not surprising that when M=0, much of the cross-section is bound by the limit determined from translational Mechanism C, particularly when $k_{\rm S}=k$. The load combination favoring surface sliding is demonstrated by the straight-line segments starting from the origin of the load space (M=0).

5.3. Factor N_{γ} for spread footings

This study focuses on the resistance of granular foundation soils to loads, owed to the weight of the soil. The results illustrated as yield loci can be interpreted in terms of resistance factor N_{γ}^{s} . This factor is used in calculations of the last component of the three-term bearing capacity formula for spread footings

$$p_{\gamma} = \frac{1}{2} \gamma B N_{\gamma}^{s} \tag{8}$$

Superscript s is used to indicate that this factor accounts for the non-

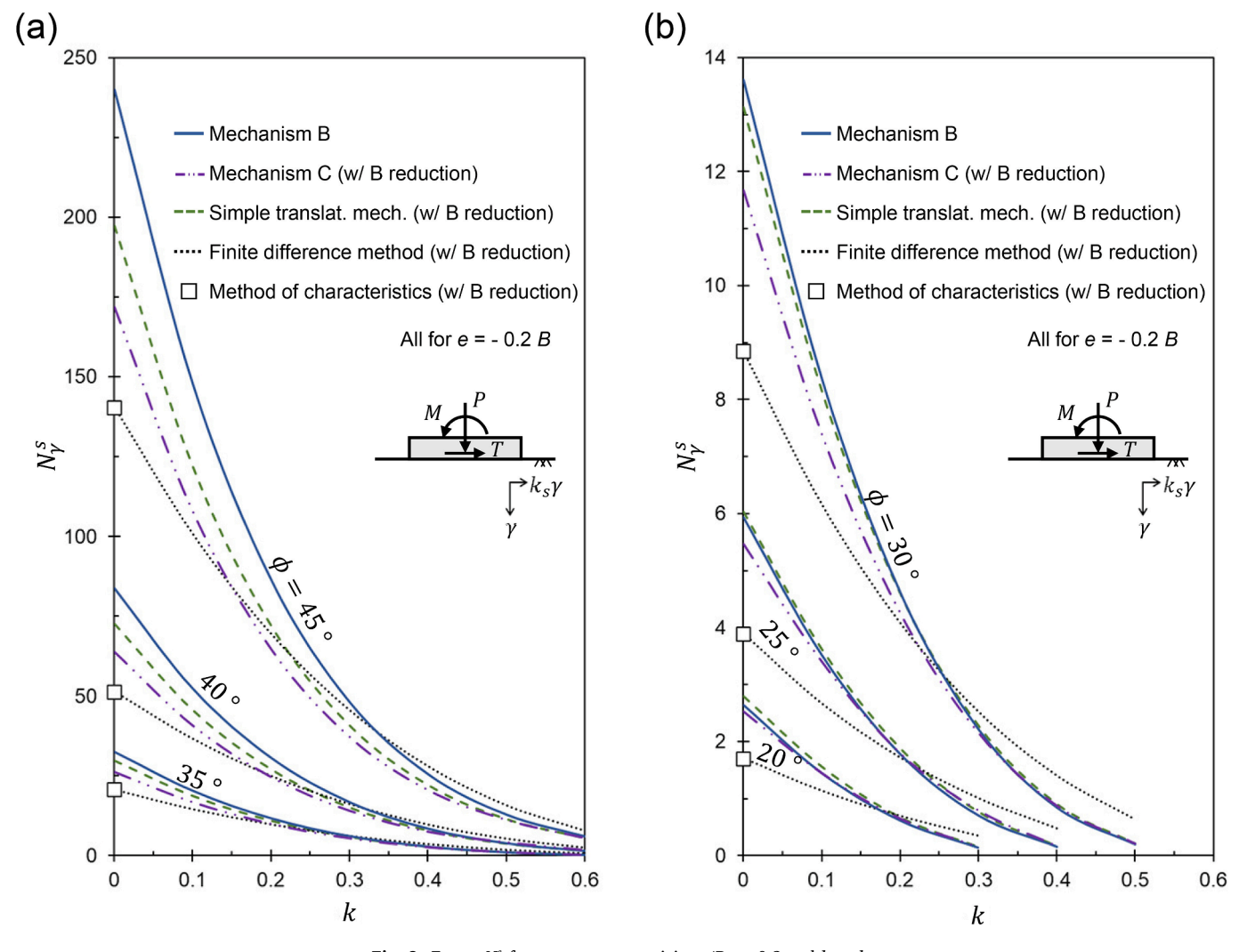


Fig. 8. Factor N_{γ}^{s} for constant eccentricity e/B= - 0.2 and $k_{s}=k$.

symmetric loads caused by seismic excitation. All charts will be presented for horizontal seismic coefficient k applied to the superstructure and equal in value coefficient k_s applied to the soil ($k_s = k$).

Earlier efforts to assess seismic bearing capacity did not focus on the moment load. Therefore, when comparing the results Meyerhof's hypothesis will be used, which suggests that the footing width be reduced by double eccentricity to account for the moment. The use of this hypothesis will be termed the "B-reduction" method. For some cases this hypothesis can be derived from purely mechanical considerations (Michalowski & You 1998b).

The first set of results is shown in Fig. 7. The two charts show factor N_{ν}^{s} as a function of average seismic coefficient k defined in Eq. (2), for an internal friction angle of the soil ranging from 45° down to 20° . Eccentricity was taken as e/B = 0.2 in calculating all results in Fig. 7, and the seismic coefficient applied to soil $k_s = k$. This is the case where both the moment and the horizontal force are positive, i.e., seismic coefficient k and eccentricity e are also both positive. Of all results presented in Fig. 7 only the limit analysis based on Mechanism A is sensitive to the moment load. The remaining four solutions are not dependent on the moment load, and to make them comparable to the Mechanism A solution, all were modified by Meyerhof's hypothesis of B-reduction. The other four solutions are: (1) the one based on Mechanism C, (2) a simple translational mechanism consisting of an assembly of triangular blocks (Michalowski, 1997, Soubra, 1999), (3) finite difference method (FLAC) as reported by Pane et al. (2016), and (4) the method of characteristics as reported by Martin (2005), though available only for k = 0. It appears

that Mechanism A yields the least solution to seismic factor N_{γ}^{s} , despite using the B-reduction method for all other solutions.

The set of results in Fig. 8 differs from that in Fig. 7 in that the moment is now negative. Mechanism B now yields better results than Mechanism A does, but overall, it is the finite difference method (Pane et al., 2016) with the B-reduction hypothesis that yields best results for low values of seismic coefficient k, whereas for higher values of k, Mechanism C with the B-reduction and Mechanism B yield least upper bounds to factor N_{γ}^{s} . The method of characteristics results are available only for k=0 (Martin, 2005), and they are consistent with the finite difference method.

The charts in Fig. 9 represent Factor $N_{\gamma}^{\rm s}$ for given k=0.3 and positive moment with e/B ranging up to 0.4, and in Fig. 10 for negative moment with e/B ranging from 0 to -0.4. When the horizontal force and the moment are both positive, Fig. 9, the best solution is obtained from Mechanism C with the B-reduction method when the eccentricity is small (typically when e/B < 0.1 and $30^{\circ} < \phi < 45^{\circ}$), and Mechanism A yields the least (best) solution for larger eccentricities. Not surprisingly, all cases where the B-reduction procedure was used show a linear dependency of $N_{\gamma}^{\rm s}$ on eccentricity e/B. This is because in the presence of a moment load Meyerhof's hypothesis requires reduction of the footing width by 2e, which produces the linear relationship of the bearing capacity factor $N_{\gamma}^{\rm s}$ on eccentricity e. When the horizontal force is positive and the moment is negative, Fig. 10, then Mechanism C with the B-reduction method yields the least solution for small eccentricities, and

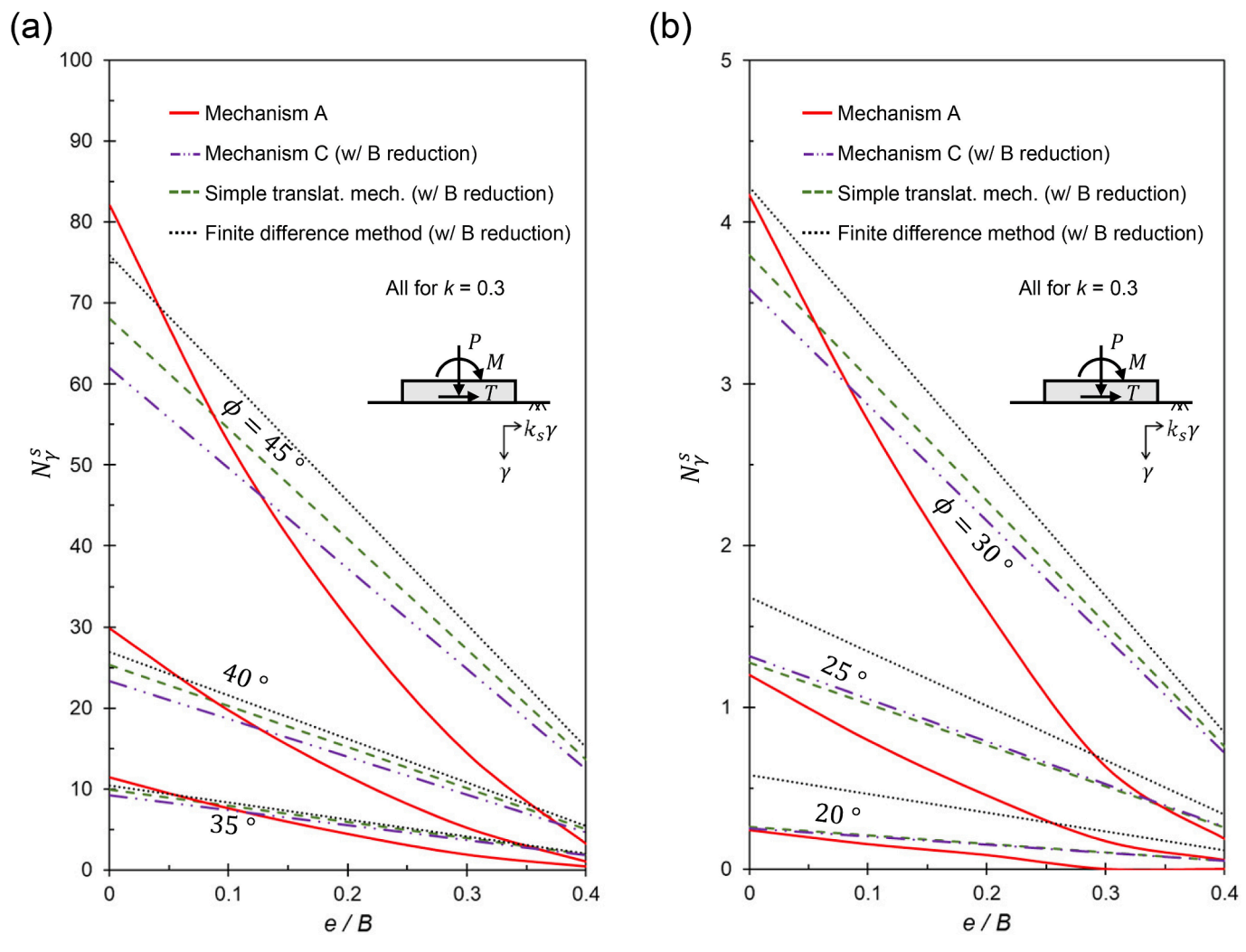


Fig. 9. Factor N_{ν}^{s} for constant k=0.3 and e>0 ($k_{s}=k$).

Mechanism B appears to yield the least results for larger eccentricities. Finally, in the absence of moment load (M=0 line in Fig. 1(b)), the best (least) solution to $N_{\gamma}^{\rm s}$ is found from the finite difference method (Pane et al., 2016) for low magnitudes of seismic coefficient k, and from limit analysis with Mechanism C for larger values of k, Fig. 11. It is surprising, however, that Mechanism A which accounts for rotation of the footing, becomes competitive when seismic coefficient becomes relatively large, e.g., k>0.36 and $\phi=30^\circ$. This point was also raised when the yield locus in Fig. 6(a) was discussed.

5.4. Comments on accuracy and finite element limit analysis approach

An analytical approach in limit analysis, explored in this paper, has been successful in solving many stability problems in geotechnical engineering (e.g., Chen, 1975). In the last decades a finite element approach implemented in limit analysis has become widely utilized. First introduced by Lysmer (1970), this approach was discussed in more detail by Sloan (2013) in his 2011 Rankine Lecture. Advantages of this method are in a larger flexibility when considering non-homogeneous soils and complex geometries, in an ease in providing both the upperand the lower-bound solutions, and in being better suited to three-dimensional collapse mechanisms. Comparison of early upper-bound bearing capacity results of strip footings on two-layer clays using both the finite element and the analytical approach showed that more accurate results are found by one method or the other, depending on the specific soil parameters and problem geometry (Merifield et al., 1999;

Michalowski, 2002). Calculations of the upper-bound bearing capacity factor N_v presented by Sloan & Yu (1996) revealed substantially higher upper-bound values than those from Mechanism C offered in this paper; for example, for $\phi = 30^{\circ}$, Mechanism C with 150 blocks yields $N_{\gamma} =$ 16.474 vs. about 20, read from the chart in Sloan & Yu (1996). Mechanism C introduced in this paper yields the best value of the analyticalapproach upper-bound limit analysis to date. Sloan & Yu used a model with 800 elements in their calculations; for the purpose of comparison the authors recalculated this example for $\phi=30^\circ$ using the finite element limit analysis Optum G2 model with 100k elements (OptumCE, 2024), and obtained a value of 15.246 for upper-bound N_{γ} , and a lowerbound value of 14.722. Not surprisingly, the finite element-based outcome depends very much on the number of elements used and adjusting the mesh (re-meshing) to the problem at hand. This upper bound is more than 20 % better than the early one in Sloan & Yu (1996), but only 7 % better than the one found using Mechanism C.

In order to shed some light on accuracy and the similarity of mechanisms used in the analytical approach and those generated using the finite-element approach, two examples are presented for seismic load cases A and D (Fig. 1(b)). The bearing capacity is sought for a strip footing on granular soil with a shear angle of $\phi=35^\circ$, no cohesion, but with overburden q given as $q/\gamma B=2.0$. Considering overburden in the analysis required the work rate of the overburden to be included in the work rate balance equation. This analysis involved simultaneous calculation of bearing capacity due to soil weight and overburden, unlike the typical separate calculations of components with cohesion,

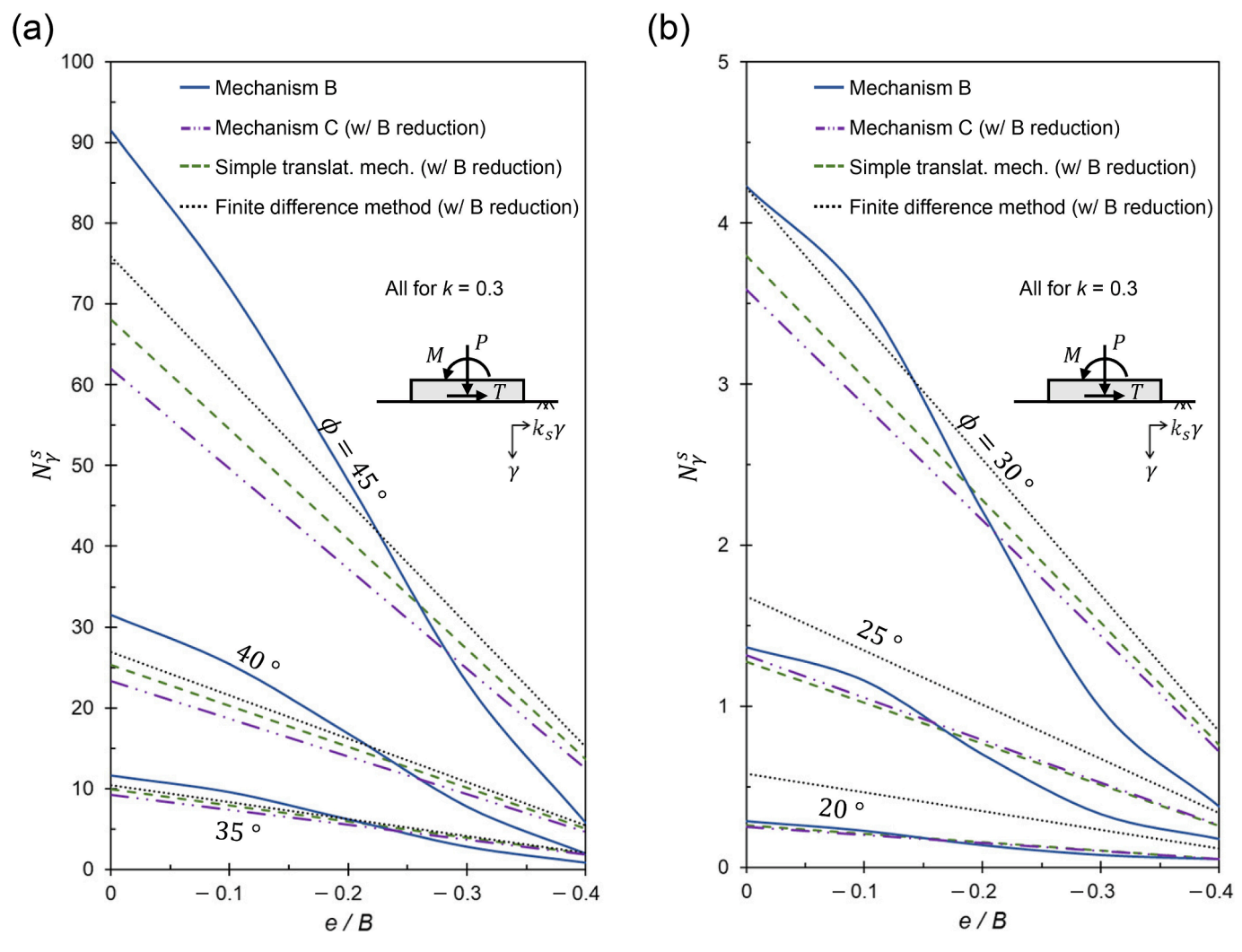


Fig. 10. Factor N_v^s for constant k = 0.3 and e < 0 ($k_s = k$).

overburden, and foundation soil weight. For Case A loading, the horizontal seismic coefficient k = 0.3 is applied to the soil, the superstructure, and overburden load q, and the load eccentricity is e = 0.2B; k =-0.3 for Case D. The shear strains in the velocity field generated by Optum G2 are shown in Fig. 12(a) with red indicating the maximum shear strain rates and dark blue being zero. The color scale indicates distinct features in the velocity field, but the magnitudes of shear strain rates are meaningful only when compared to the rate of loads (not indicated here). The contours of the velocity field in the analytical approach is shown in Fig. 12(b) (Mechanism A from Fig. 2), but with superimposed relative velocities from the Optum G2 solution. These velocities are consistent with those in the mechanism in Fig. 2(a), illustrated also in the hodograph, Fig. 2(b). It may be worth noticing that the velocity discontinuity separating the moving soil from the soil at rest is somewhat diffused in the finite-element approach, while it is a strong discontinuity in the analytical approach. Mechanism A yields the dimensionless average bearing capacity of $p/\gamma B=21.621$, whereas the upper-bound outcome from Optum G2 was found to be 21.435 (100k elements), a difference of less than 1 %. A difference of a little more than 4 % was obtained using the numerical lower-bound approach: $p/\gamma B =$ 20.710.

The second comparative example is loading Case D, with seismic coefficient of k= -0.3, all other data the same. The shear strain rates from Optum G2 are shown in Fig. 13(a) indicating a band of localized shear starting from one corner of the footing, separating the moving soil from the ground at rest. Another shear band extends from the second

corner and separates two rigid blocks. This is quite consistent with kinematic discontinuities in Mechanism B occupying about the same geometric location as the shear bands found in the finite element approach. Of the three mechanisms considered in this paper Mechanism B yields the best upper bound for loading Case $D_s p/\gamma B=24.614$, vs. $p/\gamma B=23.953$ found from the finite element approach (100 k elements), with a roughly 2.5 % difference. The finite element lower-bound outcome was $p/\gamma B=23.510$. Comparison of results in this section indicates that while the finite element limit analysis approach using a substantial number of elements and mesh adaptive technique yields slightly better results, both approaches are acceptable for geotechnical engineering purposes.

6. Conclusions

- A three-mass model of the superstructure considered provides a
 wealth of possible seismic loads on foundation soils, and it was found
 useful when interpreting the quasi-static loads owed to seismic
 excitation. However, moments produced by seismically excited superstructures and transferred to the foundation soil cannot be
 determined with confidence without dynamic analysis of the
 structure.
- A yield locus of a strip footing can be effectively produced in the space of generalized loads by considering a variety of failure modes.
 Contrary to typical procedures assuming a cigar-shaped loci, the yield locus developed in the paper is not smooth, it contains singular

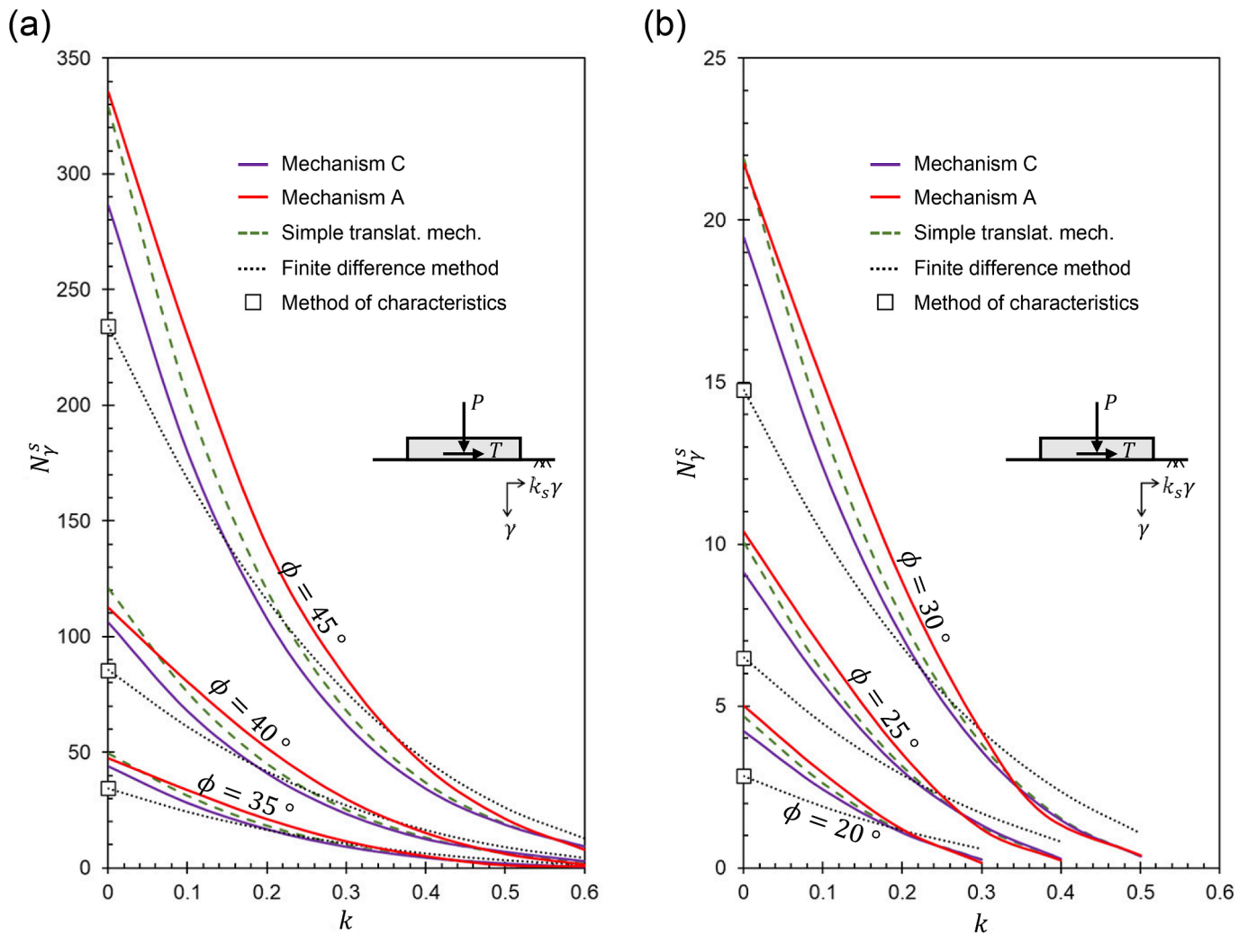


Fig. 11. Comparison of least solutions N_{γ}^{s} in the absence of moment load $(k_{s} = k)$.

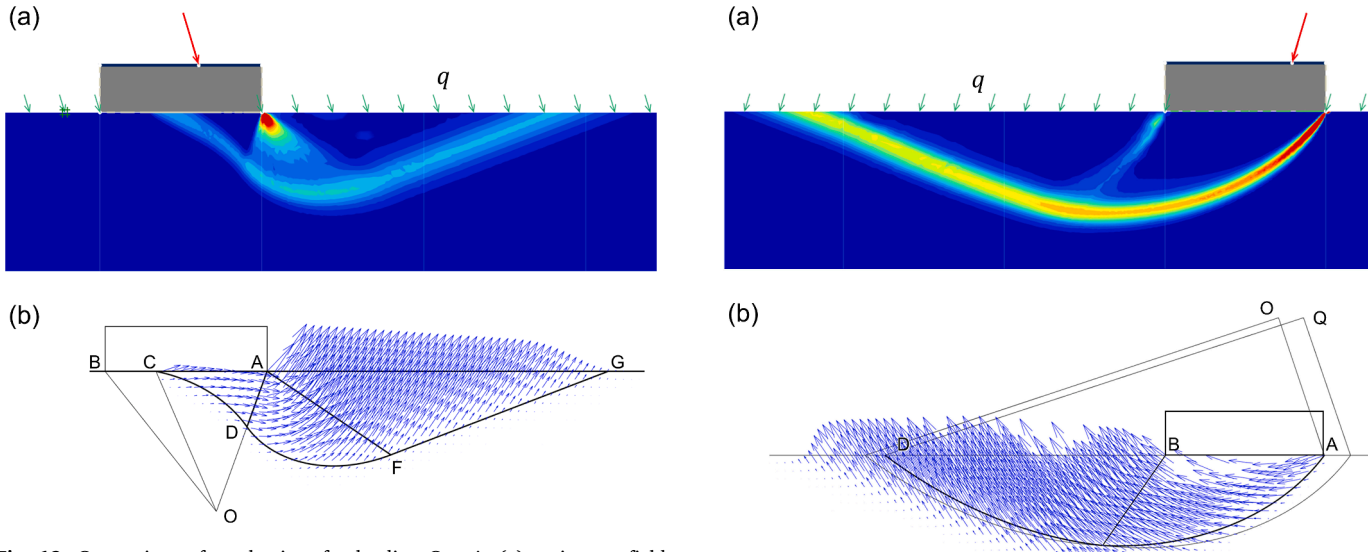


Fig. 12. Comparison of mechanisms for loading Case A: (a) strain rate field from finite element approach (red/blue - max/min), and (b) contours of optimized Mechanism A with superimposed velocities from the finite element limit analysis.

Fig. 13. Comparison of mechanisms for loading Case D: (a) strain rate field from finite element approach (red/blue - max/min), and (b) contours of optimized Mechanism B with superimposed velocities from the finite element limit analysis.

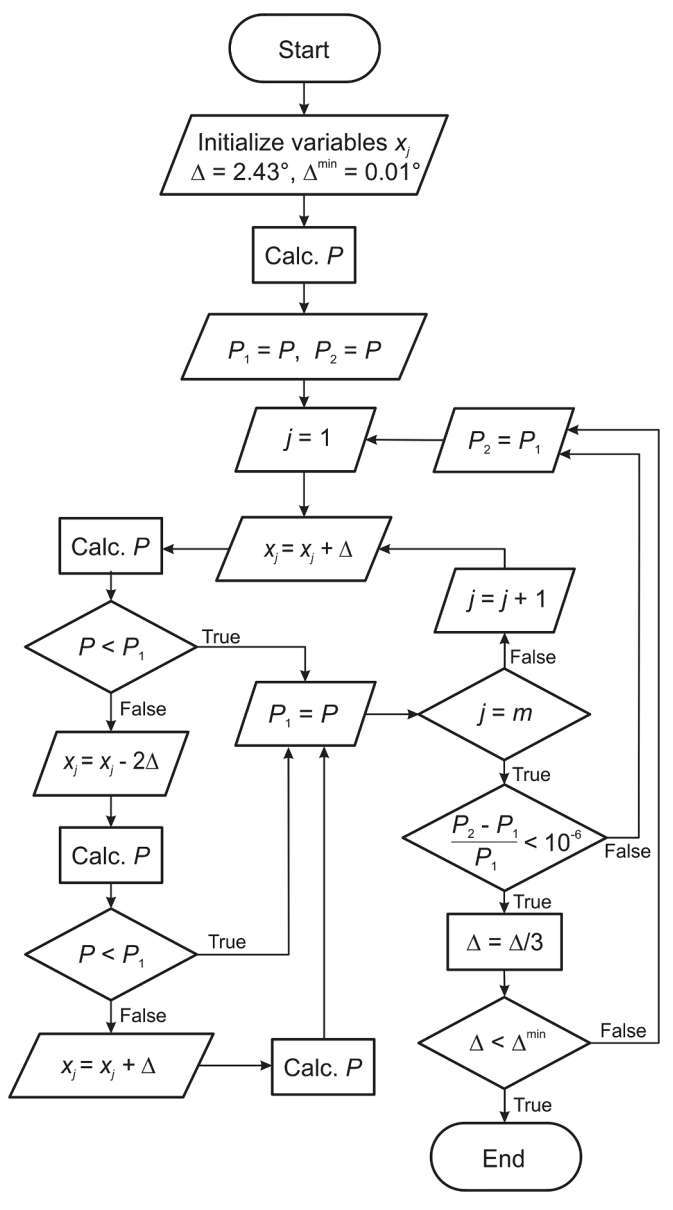


Fig. 14. Flowchart for minimization of force P.

edges (and points) indicating load combinations where a change of failure mode is permissible. The limit load surface, or the yield locus, constitutes a potential for footing permanent displacement and rotation

Of the three mechanisms used in the analysis two have novel elements. Mechanism B is a *dual-rotation* pattern with two rotating blocks separated by a planar kinematic discontinuity. This mechanism produces favorable results when the moment and the horizontal

force on the footing are of opposite sign (in the coordinate system used). The authors are not aware of the dual-rotation mechanism having ever been used in the subject literature. Mechanism C has translational kinematics and it is a significant improvement over the mechanisms used earlier in limit analysis.

• The primary outcome of the study are the solutions to bearing capacity factor N_s^s for different combinations of gravity load, the seismic horizontal force and the moment. When using kinematic limit analysis and considering moment load, the footing must undergo plastic rotation, otherwise, the mechanism will not be sensitive to the moment load. Using Meyerhof's (B-reduction) hypothesis is one way to adapt moment-insensitive solutions to moment loads. The results from three mechanisms used in this paper were compared to the outcomes from the finite difference method, limit analysis with a simple translational mechanism, and the method of characteristics available in the literature. The limit analysis outcome with Mechanism A yields the best (least) results in terms of N_x^s for the widest range of combination of non-symmetric (here seismic) loads, and so does Mechanism C with the B-reduction procedure. Mechanism B yields the best N_x^s in a limited range of load combination where the seismic horizontal force and the moment are of opposite signs, the average seismic coefficient is relatively high, and the magnitude of vertical load eccentricity is larger than 0.2 (or algebraically smaller than -0.2). Translational Mechanism C (with the B-reduction procedure) gives best results among all solutions for small moment loads. The finite difference method appears to be giving the best solutions when seismic horizontal force and moment are of opposite signs and when seismic coefficient k is low. There is no one mechanism that would yield the best solution for all load combinations.

CRediT authorship contribution statement

Yeon Sam Kim: Investigation, Formal analysis. **Radoslaw L. Michalowski:** Writing – original draft, Supervision, Conceptualization.

Declaration of competing interest

The authors declare that they have no known competing financial interests or personal relationships that could have appeared to influence the work reported in this paper.

Data availability

No data was used for the research described in the article.

Acknowledgement

The work presented in this paper was supported by the National Science Foundation, Grant No. CMMI-1901582. This support is greatly appreciated. The authors also would like to thank Prof. Kristian Krabbenhoft and Optum Computational Engineering for the academic license of Optum G2.

Appendix A

Implementing Mechanism B in limit analysis

Recognizing that the results in the paper are illustrated only for a rough grid of parameters, additional details are provided about the calculation procedure for Mechanism B, in the hope that readers might find it useful in developing their own tools when in need of more comprehensive results. For a more detailed description of Mechanism A, readers are encouraged to read papers by Paolucci & Pecker (1997) and Michalowski & You (1998a), whereas remarks on construction of multi-block mechanisms, such as that in Mechanism C, can be found in Chen (1975).

The upper bound to the bearing capacity is calculated from inequality (1), written here algebraically as

$$0 > W_P + W_v \tag{9}$$

where W_P and W_γ are the work rates of vertical limit force P and soil weight, respectively. The left-hand side of inequality (1) is zero as a consequence of the absence of the cohesive component of the strength. Introducing geometrical quantities

$$r_0 = \overline{OA}$$

$$r_h = \overline{OC} = r_0 e^{(\theta_h - \alpha_1) \tan \phi}$$
 (10)

$$l = \overline{OB} = r_0 \frac{\sin \alpha_1}{\sin \beta_1}$$

the rate of work of the limit load on the footing can be calculated from the following expression

$$W_P = P\omega \left[\frac{B}{2} - l(\cos\beta_1 + k\sin\beta_1) + e \right]$$
(11)

where the limit combination of loads is: P, T = Pk, M = Pe. Symbol ω is the angular velocity about points O and Q, B is the footing width, e is the eccentricity of vertical load P, and angle β_1 is marked in Fig. 3. Referring again to Fig. 3, the second term in inequality (9) can be found as the sum of the work rates of the two rigid rotation regions: ACBA and DCBD. In region ACBA the work of gravity and seismic work can be calculated as

$$W_{\gamma}^{ACBA} = W_{\gamma}^{ACOA} - W_{\gamma}^{ABOA} - W_{\gamma}^{BCOB} \tag{12}$$

with

$$W_{ACOA} = \omega \gamma r_0^3 (f_1 + k_s f_1^s)$$

where k_s is the seismic coefficient for the soil, and

$$f_{1} = \frac{1}{3(1 + 9\tan^{2}\phi)} \left[(3\tan\phi\cos\theta_{h} + \sin\theta_{h})e^{3(\theta_{h} - \alpha_{1})\tan\phi} - 3\tan\phi\cos\alpha_{1} - \sin\alpha_{1} \right]$$

$$f_{1}^{s} = \frac{1}{3(1 + 9\tan^{2}\phi)} \left[(3\tan\phi\sin\theta_{h} - \cos\theta_{h})e^{3(\theta_{h} - \alpha_{1})\tan\phi} - 3\tan\phi\sin\alpha_{1} + \cos\alpha_{1} \right]$$

$$(13)$$

Introducing the Cartesian coordinate system at point O (Fig. 3(a)) and defining the centroids of areas ABOA and BCOB as $(\bar{x}_{ABOA}, \bar{y}_{ABOA})$ and $(\bar{x}_{BCOB}, \bar{y}_{BCOB})$, the last two terms in Eq. (12) can be calculated as

$$W_{\gamma}^{ABOA} = \omega \gamma (\bar{\mathbf{x}}_{ABOA} + k_s \bar{\mathbf{y}}_{ABOA}) A_{ABOA}$$

$$W_{\gamma}^{BCOB} = \omega \gamma (\bar{\mathbf{x}}_{BCOB} + k_s \bar{\mathbf{y}}_{BCOB}) A_{BOCB}$$
(14)

In a similar manner, work rate W_{γ}^{DCBD} in region DCBD can be calculated. Utilizing Eq. (9), the upper bound to limit load P is found as

$$P = -\frac{W_{\gamma}^{ACBA} + W_{\gamma}^{DCBD}}{\omega \left[\frac{B}{2} - l(\cos\beta_1 + k\sin\beta_1) + e \right]}$$

$$(15)$$

Minimization of force P

Expressions in Eqs. (6), (7) and (15) were used in computations of the footing yield locus in space P, T, M. As the loading was reduced to one-parameter loading, the limit value of vertical load P was calculated first, and associated limit values of T and M were determined from: T = P k and M = Pe, as per Eq. (2) (see also Eq. (5)). The procedure starts from constructing the first kinematically admissible mechanism of type A, B or C. This involves assuming the first set of admissible independent variables; for example, for Mechanism A these are angles A, A, and A. Next, these independent variables are altered sequentially, one-by-one, by increment A until the minimum of calculated force A is reached. Each time a single independent variable is altered, the kinematic admissibility of the mechanism must be reevaluated. This process is illustrated in the flowchart in Fig. 14. Symbol A in the flowchart denotes A independent variables in the mechanism.

In this process of minimization, increment Δ was reduced from its maximum (initial value) of 2.43° to the minimum of 0.01° in 5 three-fold reduction steps. Mechanism B is fully defined by four independent variables (α_1 , β_1 , α_2 , β_2), but Mechanism C has a larger number of independent variables, as it includes a substantial number of kinematic discontinuities (interfaces between the blocks), and each linear segment of a discontinuity is defined by an independent variable angle of inclination. The number of independent variables in Mechanism C is dependent on the number of blocks, and an expression for the number of variables was developed in the previous Section.

References

- Bransby, M., Randolph, M., 1998. Combined loading of skirted foundations. Géotechnique 48 (5), 637-655.
- Cascone, E., Casablanca, O., 2016. Static and seismic bearing capacity of shallow strip footings. Soil Dyn. Earthq. Eng. 84, 204-223.
- Chen, W.-F., 1975. Limit analysis and soil plasticity. Elsevier, New York.
- Dormieux, L., Pecker, A., 1995. Seismic bearing capacity of foundation on cohesionless soil. J. Geotech. Eng.-ASCE 121 (3), 300-303.
- Gazetas, G., Garini, E., Anastasopoulos, I., Georgarakos, T., 2009. Effects of near-fault ground shaking on sliding systems. J. Geotech. Geoenviron. Eng. 135 (12), 1906-1921.
- Gottardi, G., Butterfield, R., 1993. On the bearing capacity of surface footings on sand under general planar loads. Soils Found. 33 (3), 68-79.
- Keverling Buisman, A. S. 1940. Grondmechanica, Waltman, Delft.
- Koiter, W.T., 1953. Stress-strain relations, uniqueness and variational theorems for elastic-plastic materials with a singular yield surface. Q. Appl. Math. 11 (3), 350-354.
- Lysmer, J., 1970. Limit analysis of plane problems in soil mechanics. J. the Soil Mech. Foundat. Div. 96 (4), 1311-1334.
- Martin, C., 2005. Exact bearing capacity calculations using the method of characteristics. Proc. IACMAG. Turin 11, 441-450.
- Merifield, R., Sloan, S., Yu, H., 1999. Rigorous plasticity solutions for the bearing capacity of two-layered clays. Géotechnique 49 (4), 471-490.
- Michalowski, R.L., 1997. An estimate of the influence of soil weight on bearing capacity using limit analysis. Soils Found. 37 (4), 57-64.
- Michalowski, R.L., 2002. Collapse loads over two-layer clay foundation soils. Soils Found. 42 (1), 1–7.
- Michalowski, R.L., You, L., 1998a. Non-symmetrical limit loads on strip footings. Soils Found. 38 (4), 195-203.

- Michalowski, R.L., You, L., 1998b. Effective width rule in calculations of bearing capacity of shallow footings. Comput. Geotech. 23 (4), 237-253.
- Narita, K., Yamaguchi, H., 1989. Analysis of bearing capacity for log-spiral sliding surfaces. Soils Found. 29 (2), 85-98.
- Nova, R., Montrasio, L., 1991. Settlements of shallow foundations on sand. Géotechnique
- 41 (2), 243–256. Optum^{CE} 2024. "Optum G2. Optum Computational Engineering. https://optumce.com/ products/optumg2/.
- Pane, V., Vecchietti, A., Cecconi, M., 2016. A numerical study on the seismic bearing capacity of shallow foundations. Bull. Earthq. Eng. 14, 2931-2958.
- Paolucci, R., Pecker, A., 1997. Seismic bearing capacity of shallow strip foundations on dry soils. Soils Found. 37 (3), 95-105.
- Pender, M., 2018. Earthquake inertia effects on shallow foundation bearing strength. Géotechnique 68 (7), 640-645.
- Prager, W. 1959. An Introduction to Plasticity, Addison-Wesley, Reading, Massachusetts,
- Richards Jr, R., Elms, D., Budhu, M., 1993. Seismic bearing capacity and settlements of foundations. J. Geotech. Eng.-ASCE 119 (4), 662-674.
- Salençon, J., Pecker, A., 1995. Ultimate bearing capacity of shallow foundations under inclined and eccentric loads. Part I: purely cohesive soil. Eur. J. Mech., Series A Solids 14 (3), 349-375.
- Sarma, S., Iossifelis, I., 1990. Seismic bearing capacity factors of shallow strip footings. Géotechnique 40 (2), 265-273.
- Sloan, S., 2013. Geotechnical stability analysis. Géotechnique 63 (7), 531-571.
- Sloan, S.W., Yu, H.S., 1996. Rigorous Plasticity Solutions for the Bearing Capacity Factor Ny. In: 7th Australia New Zealand Conference on Geomechanics: Geomechanics in a Changing World: Conference Proceedings. Institution of Engineers, Australia, Barton, ACT, pp. 544-550.
- Soubra, A.-H., 1999. Upper-bound solutions for bearing capacity of foundations. J. Geotech. Geoenviron. Eng. 125 (1), 59-68.
- Terzaghi, K., 1943. Theoretical Soil Mechanics. Wiley, New York.